Non Uniform Multiresolution Method for Optical Flow and Phase Portrait Models: Environmental Applications

Isaac COHEN, Isabelle HERLIN

Rapport de recherche

Non Uniform Multiresolution Method for Optical Flow and Phase Portrait Models: Environmental Applications

Isaac COHEN, Isabelle HERLIN

Thème 3 — Interaction homme-machine,
images, données, connaissances
Projet AIR

Abstract: In this paper we define a complete framework for processing large image sequences for a global monitoring of short range oceanographic and atmospheric processes. This framework is based on the use of a non quadratic regularization technique in optical flow computation that preserves flow discontinuities. We also show that using an appropriate tessellation of the image according to an estimate of the motion field can improve optical flow accuracy and yields more reliable flows. This method defines a non uniform multiresolution approach for coarse to fine grid generation. It allows to locally increase the resolution of the grid according to the studied problem. Each added node refines the grid in a region of interest and increases the numerical accuracy of the solution in this region. We make use of such a method for solving the optical flow equation with a non quadratic regularization scheme allowing the computation of optical flow field while preserving its discontinuities. The second part of the paper deals with the interpretation of the obtained displacement field. We make use of a phase portrait model with a new formulation of the approximation of an oriented flow field allowing to consider arbitrary polynomial phase portrait models for characterizing salient flow features. This new framework is used for processing oceanographic and atmospheric image sequences and presents an alternative to complex physical modeling techniques.

Key-words: Non uniform Multiresolution, Optical flow, Non quadratic regularization, Finite element method, Adaptive mesh, Phase portrait, Flow pattern classification, Ocean and atmospheric circulation.

(Résumé : tsvp)

Méthode de Multi-résolution Non uniforme pour le calcul et l'interprétation du flot optique : Application aux images environnementales

Résumé : Dans cet article, nous présentons une méthode pour le traitement de séquences d'images dédiées à la caractérisation de phénomènes océanique et atmosphérique. Cette méthode est basée sur le calcul du flot optique à l'aide d'un critère de régularisation non quadratique préservant les discontinuités du mouvement. Nous montrons également que l'utilisation d'un maillage non uniforme permet l'obtention de champs de déplacement plus précis au voisinage des structures en mouvement. Cette approche permet de définir une approche multirésolution non uniforme très performante. L'insertion de nouveaux nœuds affine localement le maillage par rapport au mouvement détecté. La seconde partie de l'article décrit une méthode d'interprétation de champ de déplacement calculé. Pour cela, nous utilisons un modèle de portrait de phase polynômial permettant la caractérisation des structures du champ de vecteur. Ces méthodes sont appliquées au traitement de séquences d'images océaniques et atmosphériques pour le calcul et l'interprétation du mouvement apparent.

Mots-clé : Multirésolution non uniforme, Eléments finis, Maillage adaptatif, Portrait de phase, Classification d'un champ de vecteurs, Circulation océanique et atmosphérique

1   Introduction

The increasing number of satellites dedicated to environmental monitoring allows to characterize natural phenomena through different physical measurements. Furthermore, the regular spatial and temporal sampling allows to characterize short range evolution of atmospheric and oceanographic phenomena by processing an image sequence. For example, Sea Surface Temperature (SST), altimetic and ocean color measurements can be used simultaneously or separately for studying sea surface streams.

In this paper we define a complete framework for processing large image sequences for a global monitoring of short range oceanographic and atmospheric phenomena. Processing such image sequences for apparent motion computation in order to detect a global displacement (oceanographic stream, cloud motion,...) and to localize a particular structure like vortex or front leads to the study of:

- a new model for motion computation preserving flow discontinuities in order to model physical phenomenon like eddies,

- a non uniform multiresolution approach for coarse to fine grid generation. It allows to increment locally the resolution of the grid in regions where a motion is detected,

- an approach for approximating an orientation field and

- characterizing the stationary points of the trajectories obtained from an arbitrary polynomial phase portrait in order to handle multiple stationary points.

The first part of the paper concerns the efficient computation of optical flow field while preserving flow discontinuities. Recovering these discontinuities is necessary for further analysis of oceanographic and atmospheric images. Indeed, locating and tracking of temperature fronts in oceanographic images represent an accurate estimation of the oceanic surface circulation. These fronts are defined as regions where the spatial temperature variation is high. An accurate computation of optical flow components near these regions must take into account the motion discontinuity along the temperature front. For this purpose, we define a non quadratic regularization scheme

preserving flow discontinuities while insuring a unique solution of optical flow equation. An efficient solution is obtained through a non uniform multiresolution method defining a new approach for coarse to fine grid generation. It allows to locally increase the resolution of the grid according to the studied problem by creating a motion index. Each added node refines the grid in a region of interest and increases the numerical accuracy of the solution in this region.

The second part of the paper deals with the interpretation of the obtained displacement field. A velocity field can be studied from two different view points. First, it is a motion field and therefore it can be studied according to the analysis of fluid motion. On the other hand, it is a vector field whose topology is described by its critical points and salient features. The second approach is more suitable in our context since the characterization of salient flow features will help us in locating interesting structures like vortex and front, which represent physical phenomena appearing in SST and atmospheric image sequences. We present in this paper a new approach for approximating an orientation field and characterizing the stationary points of the trajectories obtained from an arbitrary polynomial phase portrait. This model is an extension of the commonly used linear model which can handle only one critical point. Furthermore the model is always linear, independently of the chosen polynomial representation.

The paper is structured as follows: Section 2 briefly presents a non quadratic regularization method for optical flow computation preserving flow discontinuities, its connection with the mean curvature motion model, and the Finite Element Method used for solving the nonlinear partial differential equation. Section 3 describes the non uniform multiresolution technique used for the optical flow equation. Section 4 gives some experimental results. A review of previous works on flow pattern approximation and our new formulation of polynomial orientation field approximation are presented in section 5 while section 6 describes the flow pattern classification of arbitrary polynomial phase portrait model. Illustrations and experimental results are given in the different sections to enlighten the different models we used. The experiments were led on classical synthetic image sequences to establish the accuracy of the proposed model, while oceanographic and atmospheric image sequences are used to illustrate the use of motion computation and interpretation framework for an environmental applications.

2 Non Quadratic Optical Flow Computation

The differential techniques used for computing the optical flow are based on the image flow constraint equation:

$$\frac{dI(x, y, t)}{dt} = I_x u + I_y v + I_t = 0, \tag{1}$$

where the subscripts x, y and t represent the partial derivatives. This equation, based on the assumption that the pixel gray level remains constant, relates the temporal and spatial changes of the image gray level $I(x, y, t)$ at point (x, y) to the velocity (u, v) at the same point [12]. Equation (1) is not sufficient for computing the image velocity (u, v) at each point since the velocity components are constrained by only one equation; this is the aperture problem. Therefore, most of the techniques use a regularity constraint that restrains the space of admissible solutions of equation (1) ([1] and references therein). This regularity constraint is generally quadratic and enforces the optical flow field to be continuous and smooth. But, true discontinuities can occur in the optical flow and are generally located on the boundary between two surfaces representing two objects with different movements. This type of discontinuity occurs for example on temperature front in SST images, and cloud boundary in atmospheric images. Recovering this discontinuity is necessary for further analysis of oceanographic and atmospheric images. Indeed, locating and tracking of temperature fronts in oceanographic images represent an accurate estimation of the oceanic surface circulation. These fronts are defined as regions where the spatial temperature variation is high. An accurate computation of optical flow components near these regions must take into account the motion discontinuity along the temperature front. For this purpose, we define a non quadratic regularization scheme preserving flow discontinuities while insuring a unique solution of equation (1).

2.1 Quadratic and Stochastic Models

With a quadratic regularization technique, constraining the space of admissible solutions of equation (1) leads to the minimization of the functional:

$$E(u, v) = \alpha \int_{\Omega} |\nabla u|^2 + |\nabla v|^2 \, dx dy + \int_{\Omega} (I_x u + I_y v + I_t)^2 \, dx dy, \tag{2}$$

where (u, v) are the flow field components, α is a regularization parameter and ∇ denotes the gradient operator.

The quadratic regularizer $\int_\Omega |\nabla u|^2 + |\nabla v|^2 \, dxdy$ constrains the optical flow field to be continuous. Indeed, the stationarity constraint ($\frac{dI(x,y,t)}{dt} = 0$) is not sufficient to compute the two components of the optical flow and in order to insure a unique minimum of the functional E (Eq. 2) it is necessary to choose $\alpha > 0$ and consequently the minimum is constrained to be continuous. This regularization technique (Eq. 2) is used in most cases due to its computational simplicity, since the minimization of (2) leads to solve a linear set of equations [12].

Black *et al* [3, 4] proposed several non-quadratic schemes for discontinuous motion estimation. These methods are based on the Lorentzian estimator which allows to reduce the effects of outliers (points which violates the optical flow hypothesis or the smoothness assumption) in the minimization done through a Simultaneous Over Relaxation or a Graduated Non Convexity method. These stochastics approaches can not handle non uniform tessellation of the image which is an important issue when dealing with very large image sequences as described in section 3.

2.2   Non Quadratic Variational Model

In this section we present a method for computing optical flow based on a non-quadratic regularization technique. This method makes use of the L^1 norm (defined by $|u|_1 = \int |u|$) for the regularization constraint. The advantage of this norm is that the variation of an expression like $|u|_1$ produces singular distributions as coefficients (e.g. Dirac functions). This property allows to preserve sharp signals as well as discontinuities in the space of L^1 functions. Such a property can be used to constrain the set of admissible solutions of Eq. (1). Considering the space of functions with bounded variation, i.e. :

$$BV_1 = \left\{ f = (f_1, f_2) \text{ such that } \int_\Omega |\nabla f_1| + |\nabla f_2| \, dxdy < +\infty \right\},$$

the optical flow problem can be stated as the minimization of the functional :

$$\int_\Omega \sqrt{u_x^2 + u_y^2} + \sqrt{v_x^2 + v_y^2} + (I_x u + I_y v + I_t)^2 \, dxdy, \tag{3}$$

where u_x and u_y (resp. v_x and v_y) represent the partial derivatives of u (resp. v) with respect to x and y.

This minimization problem (3) can also be viewed as a constrained minimization problem where a vector flow field have to be determined in the space of functions with bounded variation BV_1, with the constraint of satisfying the optical flow stationarity equation (Eq. (1)).

The solution of the minimization problem (3) is obtained through the Euler - Lagrange equations:

$$\begin{cases} \mathcal{D}u + (uI_x^2 + vI_xI_y + I_xI_t) = 0 \\ \mathcal{D}v + (uI_xI_y + vI_y^2 + I_yI_t) = 0 \\ +\text{Boundary conditions:} \nabla u_{|\Gamma} = \nabla v_{|\Gamma} = 0 \end{cases} \tag{4}$$

where $\mathcal{D}$ is the nonlinear operator defined by:

$$\mathcal{D}f = -\frac{\partial}{\partial x}\left(\frac{f_x}{\sqrt{f_x^2 + f_y^2}}\right) - \frac{\partial}{\partial y}\left(\frac{f_y}{\sqrt{f_x^2 + f_y^2}}\right). \tag{5}$$

Equations (4) are nonlinear and therefore must be processed in a particular way. An efficient method for solving this kind of nonlinear partial differential equation is to consider the associated evolution equations, or equivalently, the gradient descent method [9, 22]. This time-dependent approach means that the evolution equations:

$$\begin{cases} \frac{\partial u}{\partial t} + \mathcal{D}u + (uI_x^2 + vI_xI_y + I_xI_t) = 0 \\ \frac{\partial v}{\partial t} + \mathcal{D}v + (uI_xI_y + vI_y^2 + I_yI_t) = 0 \\ +\text{Boundary conditions:} \nabla u_{|\Gamma} = \nabla v_{|\Gamma} = 0 \\ +\text{Initial estimation } u(0, x, y) = u_0(x, y). \end{cases} \tag{6}$$

characterize, through a stationary solution, a solution of the initial nonlinear problem (Eq. 4).

The evolution equations may be solved with a finite difference or a finite element method. Rudin *et al* [23] proposed a finite difference method for image deblurring, by using similar equations solved over a rectangular tessellation of the image. Such a method can be used for a uniform image tessellation but cannot handle non-uniform tessellations which provide a finer resolution near moving structures.

In this paper we propose a finite element method allowing the use of arbitrary tessellation of the image domain by taking into account locations where motion occur. These locations are obtained through an index measuring the normal component of the optical flow field. This index allows to define a non uniform tessellation which reduces the numerical complexity of the algorithm and

increases its accuracy near moving structures. This is performed with the non uniform multiresolution method described in section 3. The use of a FEM gives a natural way for sampling the solution over the different grid levels by making use of the analytical representation of the solution.

Before describing the numerical solution of equation (6), we report in the next section some connections of the proposed non quadratic model with the mean curvature motion models.

2.3   Connection with the Mean Curvature Motion models

The nonlinear method, we presented in the previous section, has some strong connections to the mean curvature motion scheme. Indeed, both approaches use the non quadratic regularizer:

$$\int_\Omega |\nabla \varphi| = |\nabla \varphi|_{L^1} \tag{7}$$

where φ is the cartesian surface representation of the image (*i.e* $\varphi(x, y) = I(x, y)$) in the case of image smoothing [14, 16, 19] or the optical flow components in our approach.

The evolution equation of the mean curvature motion model is:

$$\frac{\partial \varphi}{\partial t} + \nabla \frac{\nabla \varphi}{|\nabla \varphi|} = \frac{\partial \varphi}{\partial t} + \mathcal{D}\varphi = \frac{\partial \varphi}{\partial t} + \kappa |\nabla \varphi| = 0 \tag{8}$$

where κ is the gaussian curvature of φ. This equation is closely related to the evolution scheme (6) used for solving the initial nonlinear PDE (4) which can be written as:

$$\frac{\partial w}{\partial t} + \mathcal{D}w = -\nabla I \left(\nabla I^t w + I_t \right). \tag{9}$$

It represents a nonlinear smoothing by curvature deformation of the surface $w = (u, v)$ defined by the flow components. The proposed model forces the solution to verify the optical flow constraint equation (second term of equation (9)), and has consequently a non trivial stationary state, eliminating therefore the problem of choosing a stopping time for the evolution equation.

This similarity between the two models allows to derive theoretical results such as the annihilation of extrema and inflection points and the semi-group property [14].

2.4   Finite Element Solution

The solution of the partial differential equation (6) cannot be obtained through a classical finite element method (FEM) since it is nonlinear. In the following, we present an iterative method for

solving this equation. This scheme is based on successive linear approximations of the differential operator $\mathcal{D}$.

Let us consider the following representation of the evolution equation (6):

$$\frac{\partial w}{\partial t} + \mathcal{D}w + \nabla I \nabla I^T w = -\frac{\partial I}{\partial t} \nabla I \tag{10}$$

where $w = (u, v)^T$ represents the flow field components and $\nabla I = (I_x, I_y)^T$ the image derivatives.

The iterative linear approximation of the nonlinear operator $\mathcal{D}$ is based on the following semi-implicit discretization scheme:

$$\frac{w^n - w^{n-1}}{\tau} + \mathcal{D}_n w^n + \nabla I \nabla I^T w^n = -\frac{\partial I}{\partial t} \nabla I \tag{11}$$

where τ is the time step, $w^n = w(x, y, n\tau)$ and $\mathcal{D}_n$ is defined by :

$$\mathcal{D}_n f = -\frac{\partial}{\partial x}\left(\frac{f_x^n}{\sqrt{(f_x^{n-1})^2 + (f_y^{n-1})^2}}\right) - \frac{\partial}{\partial y}\left(\frac{f_y^n}{\sqrt{(f_x^{n-1})^2 + (f_y^{n-1})^2}}\right).$$

This time discretization scheme is unconditionally stable, *i.e.* the convergence of the sequence f^n to a stationary solution f (*i.e.* $\frac{\partial f}{\partial t} = 0$) does not depend on the time step value τ. Such a scheme allows us to define the following time dependent variational problem:

$$a_n(w^n, g) = L(g); \qquad \forall g \in H^1(\Omega) \tag{12}$$

where:

$$a_n(w^n, g) = \int_\Omega \frac{1}{\sqrt{(w_x^{n-1})^2 + (w_y^{n-1})^2}} \nabla w \nabla g \, dx dy + \int_\Omega \nabla I \nabla I^T w g \, dx dy \tag{13}$$

is a bilinear form (since the upper script $(n-1)$ refers to the solution obtained at time step $(n-1)$ and may be considered as a particular weighting function at time step n), and:

$$L(g) = -\int_\Omega \frac{\partial I}{\partial t} \nabla I g \, dx dy \tag{14}$$

is a linear form. This variational problem has a unique solution since the form a_n is $H^1(\Omega)$-elliptic and consequently, a solution of the nonlinear PDE (4) is characterized through a stationary solution of the evolution equation:

$$\begin{cases} \left(\frac{\partial w}{\partial t}, g\right) + a_n(w, g) = L(g), \quad \forall g \in H^1(\Omega), \\ w(x, y, 0) = w^0(x, y) \quad \text{initial estimate} \end{cases} \tag{15}$$

Up to now we have used continuous equations with regard to the space variables (x, y). We use a Finite Element Method (FEM) for defining the discrete approximation of the nonlinear partial differential equation (6).

A FEM method is based on the Galerkin approximation of the Hilbert space $H^1(\Omega)$ over which equation (15) is defined. This space is approximated using the polynomial functions:

$$P_1(\mathbb{R}^2) = \{p(x, y) \ \ st \ \ p(x, y) = a_0 + a_1 x + a_2 y\}$$

defined over triangular patches of a given tessellation $\mathcal{T}$ of $\Omega = \bigcup_k \mathcal{T}_k$, where $\mathcal{T}_k$ a triangular patch of the triangulation. Let us consider the functions φ_{ij} defined on each nodal point (ih_x, jh_y) by:

$$\begin{cases} \varphi_{ij} \in P_1(\mathbb{R}^2), \\ \varphi_{ij}(ih_x, jh_y) = 1, \\ \varphi_{ij}(x, y) = 0 \ \ if \ \ (x, y) \notin \mathcal{V}_{ij}, \end{cases} \tag{16}$$

where $\mathcal{V}_{ij}$ is the triangular neighborhood of the node (i, j), *i.e.* $\mathcal{V}_{ij} = \bigcup_{k \ st \ ij \in \mathcal{T}_k} \mathcal{T}_k$. These functions may be used as basis functions of the space $P_1(\mathbb{R}^2)$, and consequently allows to represent each function $w \in H^1(\Omega)$ by :

$$w = \sum_{ij} w(ih_x, jh_y)\varphi_{ij}. \tag{17}$$

This representation allows us to derive, from equation (15) and its semi-implicit description (11), the following linear set of equations characterizing the numerical solution of equation (15):

$$(I + \tau A^n) w^n = w^{n-1} + \tau L \tag{18}$$

where A^n is a symmetric, positive definite matrix defined by $A^n_{ij,kl} = a_n(\varphi_{ij}, \varphi_{kl})$ and L is the vector defined by $L_{ij} = L(\varphi_{ij})$. Furthermore, this continuous representation of the solution allows to sample the solution over a non uniform grid when using a coarse to fine multigrid approach.

At each time step we solve a sparse linear system with a Conjugate Gradient (CG) method where the matrix A^n has to be computed at each iteration. A stationary solution $\left(\left|\frac{\partial v}{\partial t}\right| \leq 10^{-3}\right)$ is reached in typically five iterations of the scheme (18).

3 Non Uniform Multigrids

Computing an optical flow field over an image sequence using a classical approach leads to the solution of a large set of linear equations in the case of a quadratic regularizer or to an iterative solution for a non quadratic case. In both approaches space discretization (i.e. image tessellation) is an important issue since it defines the accuracy of the solution and the numerical complexity of the algorithm. The trade-off between these two criteria, accuracy and numerical complexity, retained attention of researchers working on minimization problems. For example, multi-resolution approaches based on several grid tessellations allow to start the minimization on a very rough tessellation, and increment grid tessellation as getting closer to the minimum. This is a first solution to the accuracy/numerical complexity trade-off since most of computation is made on the lower resolution while the final solution is obtained on the higher resolution by sampling the solution on the finest grid. The advantage of such an approach is that it allows a low numerical complexity and avoids local minima. However, most of the algorithms using a multi-resolution approach have a uniform coarse to fine sampling, which means that new nodes are added regardless of the problem being solved. For example, a 2×2 coarse grid yields a 4×4 grid at the first level, 8×8 grid at the second level and so on. This scheme adds nodes uniformly and regardless of the usefulness of these nodes.

In this section we propose a selective multi-resolution approach. This method defines a new approach for coarse to fine grid generation. It allows to increment locally the resolution of the grid according to the studied problem. The advantage of such a method is its lowest numerical complexity and its higher accuracy. Each added node refines the grid in a region of interest and increases the numerical accuracy of the solved problem (Equation (10) for instance) in this region.

3.1 Grid subdivision scheme

The successive grids are generated by a recursive subdivision of the triangles. Each grid will be used as a tessellation of the domain (*i.e.* the image) for solving the minimization problem. In the following, we deal with arbitrary domain tessellations.

Using a variational approach leads to the solution of the associated Euler-Lagrange equation. This equation is generally a Partial Differential Equation (PDE) solved through a FEM in order to

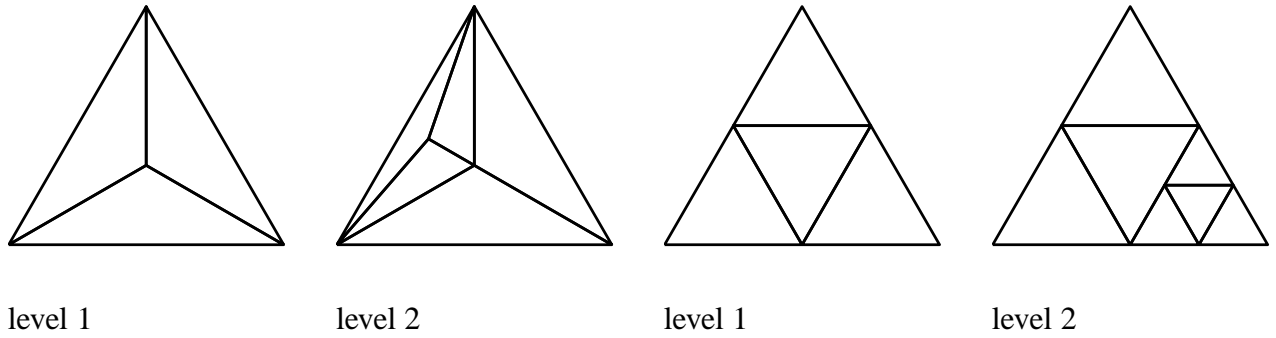level 1   level 2   level 1   level 2

Figure 1: An illustration of ternary and quaternary subdivision schemes.

take into account an arbitrary domain tessellation. This method is generic and can be used for most minimization problems but it constrains the type of admissible tessellation. The tessellation must fulfill the *conform triangulation* requirement of the FEM scheme [5], *i.e.*:

> *any face of any n-simplex $\mathcal{T}_1$ in the triangulation is either a subset of the boundary of the domain, or a face of another n-simplex $\mathcal{T}_2$ in the triangulation.*

This requirement restrains the type of n-simplex and the subdivision scheme that can be used for an automatic non-uniform cell subdivision. Indeed, different mesh refinement techniques were proposed in computer vision but most of them do not fulfill this requirement.

Hierarchical triangular decomposition methods are differentiated on the basis of whether the decomposition is into three (*ternary*) or four (*quaternary*) parts (see Figure 1). Ternary decompositions are formed by taking an internal point of one of the triangles $\mathcal{T}$ and joining it to the vertices of $\mathcal{T}$. Quaternary decompositions are formed by joining three points, each one on a different side of a given triangle. In the case of a ternary decomposition, the surface described by the triangulation is usually continuous at every level. However, the triangles are often thin and elongated : thus the equiangularity is not satisfied and this method cannot be used in a recursive scheme. Indeed, the subdivided triangles become very elongated after two or three successive subdivisions. In the case of a quaternary decomposition, each triangle can be adjacent to a number of triangles on each of its sides and the resulted surface is not continuous unless all triangles are uniformly splitted [24].

Vasilescu and Terzopoulos [27] proposed an adaptive mesh scheme for subdividing and merging elements, based on regional properties of the intensity function. But this scheme is a quaternary scheme which does not fulfill the *conform triangulation* requirement. Using such a mesh for

fitting a model to given data restricts the authors to use an additional colinearity constraint to avoid the destruction of the triangular tessellation structure.

A similar approach is based on the use of Quadtree (adaptive resolution) splines [26] *i.e.* splines defined over quadtree domains. Again, this method cannot be used in a FEM scheme since the triangulation is based on a quaternary decomposition and does not fulfill the previous conform triangulation requirement and furthermore *cracks* or first-order discontinuities in the interpolated function will arise unless a *crack-filling* strategy is used.

After reviewing the methods used for hierarchical decomposition of triangles we propose in the following a subdivision method based on triangular cells which are well adapted for domain triangulation and allow to derive a simple recursive subdivision scheme :

For each triangle $\mathcal{T}_1$ to be subdivided :

step 1 Find the adjacent triangle $\mathcal{T}_2$ sharing the largest edge of $\mathcal{T}_1$ (if this edge belongs to the domain boundary then subdivide $\mathcal{T}_2$ into two triangles),

step 2 If the shared edge is the largest edge of $\mathcal{T}_2$ then subdivide into four triangles the block $\mathcal{T}_1 \cup \mathcal{T}_2$. Otherwise process the triangle $\mathcal{T}_2$ (*i.e.* goto step 1).

This scheme is illustrated in Figure 2. The first line shows the initial triangulation where the triangle to be subdivided is gray filled and the achieved subdivision (Figure 2.b). In the second line, an example of the recursive application of the algorithm is displayed. The block $\mathcal{T}_1 \cup \mathcal{T}_2$ (Figure 2.c) cannot be subdivided since it does not fulfill the step 2 requirement, so we have to first subdivide the triangle $\mathcal{T}_2$ (Figure 2.d) before $\mathcal{T}_1$ (Figure 2.e).

3.2 A Multigrid Scheme Adapted to Motion Computation

Given a triangulation $\mathcal{T} = \bigcup_i \mathcal{T}_i$ of the image domain, we have to construct a multiresolution grid such that the grid resolution increases only near moving structures. The scheme presented in the previous section allows an optimal coarse to fine pyramid construction since the grid resolution is refined only in interesting regions. These regions are characterized as regions where a motion is detected. In the following we will prove that motion detection can be performed by using the norm
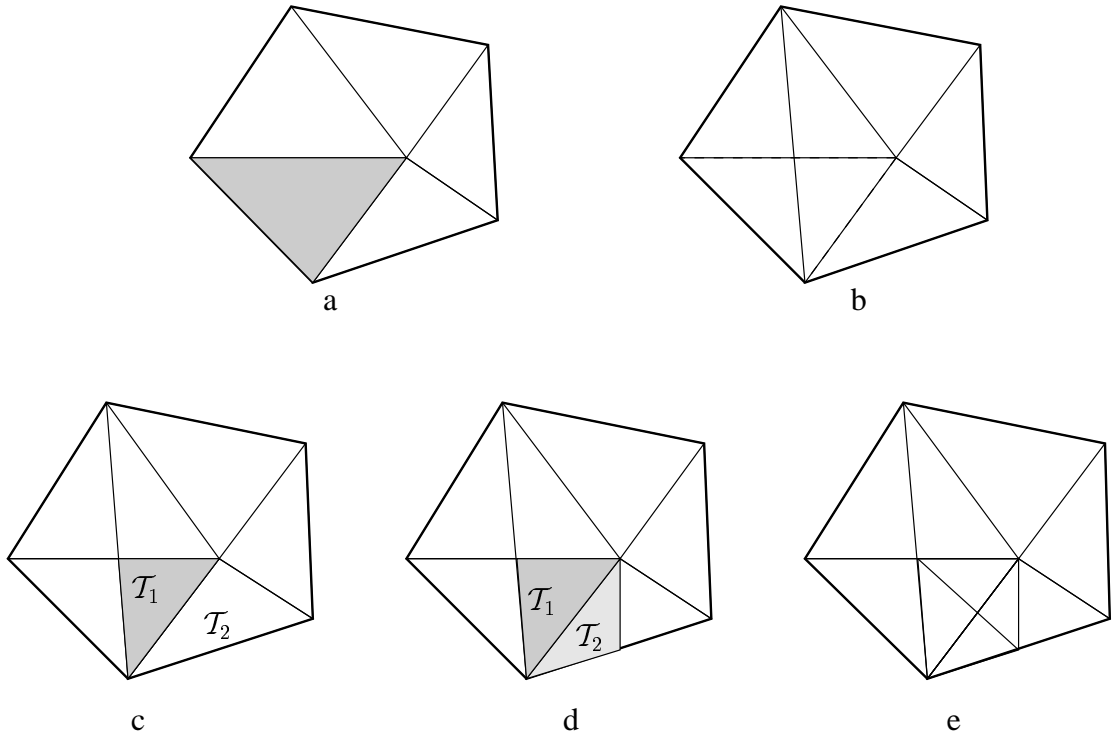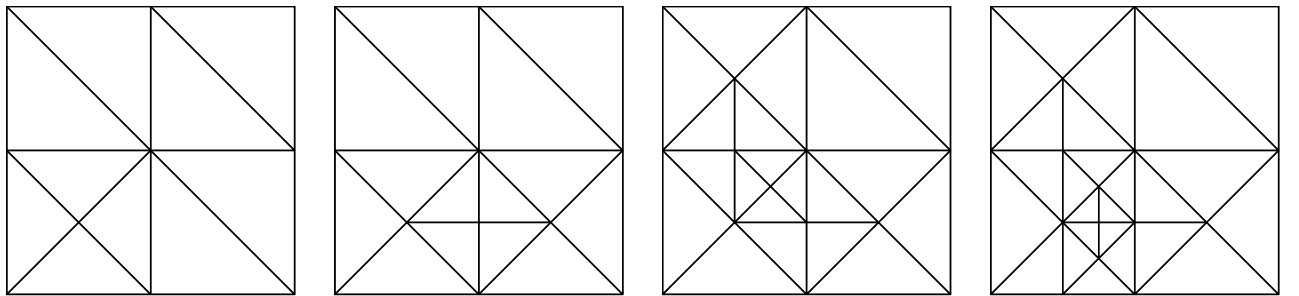
Figure 2: Illustration of the recursive subdivision scheme used to construct the different grid levels of the non uniform multigrid method. In this example, domain boundary is plotted in bold printing.

level 1   level 2   level 3   level 4

Figure 3: An illustration of the non-uniform subdivision scheme at four different levels.

of the estimated motion field along the direction of the image gradient. This normal component is used as a motion index for characterizing regions where a motion occurs.

Let I represent the image brightness and $\overrightarrow{\nabla I}$ its gradient vector field. The optical flow equation is:

$$\frac{dI}{dt} = \frac{\partial I}{\partial t} + \overrightarrow{\nabla I} . \overrightarrow{w}$$

where $\overrightarrow{w} = (u, v)$ is the optical flow. This equation can then be rewritten as [28]:

$$\frac{dI}{dt} = \frac{\partial I}{\partial t} + \|\overrightarrow{\nabla I}\| w_-$$

where w_- is the norm of the component $\overrightarrow{w_-}$ of the motion field $\overrightarrow{w}$ along the direction of $\overrightarrow{\nabla I}$.

If the flow constraint equation is satisfied (*i.e.* $\frac{dI}{dt} = 0$) and $\left\|\overrightarrow{\nabla I}\right\| \neq 0$, we obtain:

$$\overrightarrow{w_-} = -\frac{\partial I/\partial t}{\left\|\overrightarrow{\nabla I}\right\|} \frac{\overrightarrow{\nabla I}}{\left\|\overrightarrow{\nabla I}\right\|} \tag{19}$$

representing the component of the motion field along the direction of the gradient in term of the partial derivatives of I.

Although w_- does not always characterize image motion due to the aperture problem (see [12] for motion examples where equation (19) cannot characterize image motion), it allows to locate moving points. Indeed, w_- is high near moving points and becomes null near stationary points.

The definition of w_- gives the theoretical proof of the motion measure D, defined by Irani *et al* [13] and used by several authors [26, 17] :

$$D(x, y, t) = \frac{\displaystyle\sum_{(x_i, y_i) \in W} |I(x_i, y_i, t+1) - I(x_i, y_i, t)| \, |\nabla I(x_i, y_i, t)|}{\displaystyle\sum_{(x_i, y_i) \in W} |\nabla I(x_i, y_i, t)|^2 + C} \tag{20}$$

where W is a small neighborhood and C a constant used to avoid numerical instabilities. This motion measure, defined as *residual motion*, is a particular form of w_- where the numerator and the denominator are summed over a small neighborhood.

The subdivision scheme is based on a split strategy. We start with a coarse tessellation of the image and split each cell $\mathcal{T}$ of the triangulation according to the value of the norm w_- summed all over the cell: $w_-^{\mathcal{T}}$. A cell is subdivided while $w_-^{\mathcal{T}}$ is greater than a given threshold and while its area is greater than another threshold. Figure 3 illustrates a four levels subdivision scheme. This coarse to fine grid can also be used for other problems in computer vision: for example, one can use the values of $|\nabla I|^2$, instead of w_-, for a grid generation that focus on edge structures.

4   Experimental Results

We led different experimental tests on classical image sequences (see [1]); some of them are reported in the following subsections. In these experiments the temporal gradients are computed from two successive images using a smoothing gaussian operator. Increasing the number of frames yields smooth temporal gradient which is not appropriate for computing a discontinuous flow field. A final remark concerns the flow field representation: it is represented over the finest grid tessellation of the image; but we can also reconstruct the displacement field over the whole image by making use of the analytical description of the FEM solution (17). This is done for the phase portrait estimation as explained in Section 5.

4.1   Classical Image Sequences

The first example is the "rubic" [1] sequence where a Rubik's cube is rotating counter-clockwise on a turntable. We first generate the coarse to fine non uniform grids by using image spatiotemporal gradient and the algorithm described in section 3. We set the motion threshold, *i.e.* w_{-}^{T}, to one pixel/frame and the cell area threshold to 2 pixels. The obtained mesh and the resulted flow field are displayed in figure 4. We observe that the mesh resolution is finer near moving structures allowing an important reduction of the algorithmic complexity, since we deal with 340 nodes and 656 triangles, yielding an optical flow numerical accuracy lower than 0.5 pixel near moving structures. To achieve the same accuracy with a classical multigrid scheme with a rectangular mesh, one has to consider a grid with 6800 nodes. The complete processing (*i.e.* computation of the image gradients and solution of Eq. (18)) takes 20 seconds on a Alpha 3000/500 workstation.

The second image sequence is the "SRI Sequence". The camera translates parallel to the ground plane, perpendicular to its line of sight. The velocities are as large as 2 pixels/frame. Figure 5, displays the obtained flow field and the associated mesh (motion threshold w_{-}^{T} is set to 1 pixels/frame, cell area threshold to 5 pixels). We observe that while we recover a coherent flow field, the discontinuities are preserved by making use of the non quadratic scheme (Eq. 10). Furthermore the mesh tessellation is finer near flow discontinuities allowing a higher accuracy in these regions.

Finally, we have experimented our method on the "Hamburg Taxi Sequence". In this street scene, there were four moving objects at different speeds : a taxi turning the corner (1.0
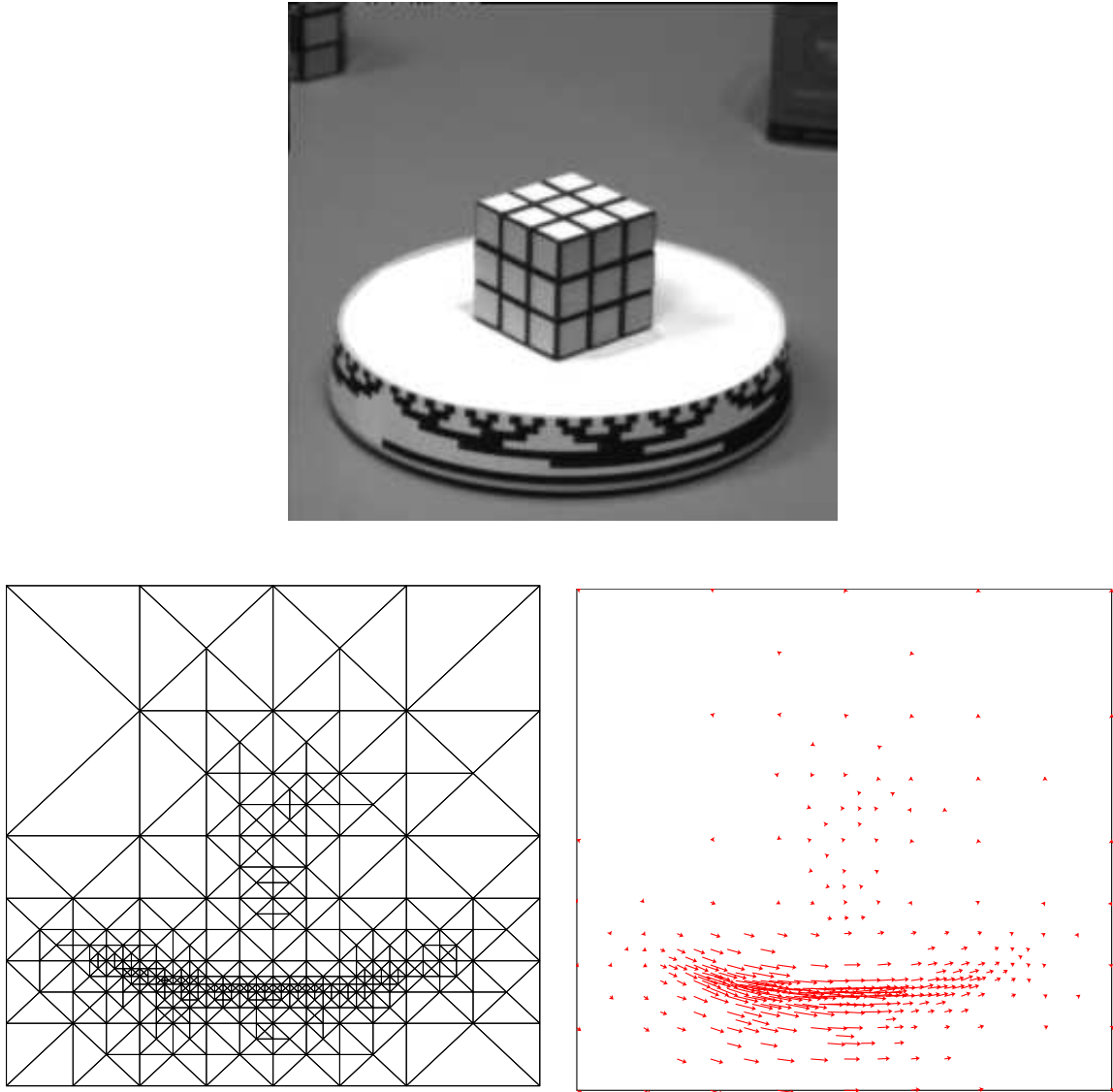
Figure 4: An illustration of the use of an adaptive mesh to increase the numerical accuracy of the computed flow field while reducing the algorithmic complexity of the method. We display a frame of the Rubik's Cube, the associated mesh and the optical flow field.
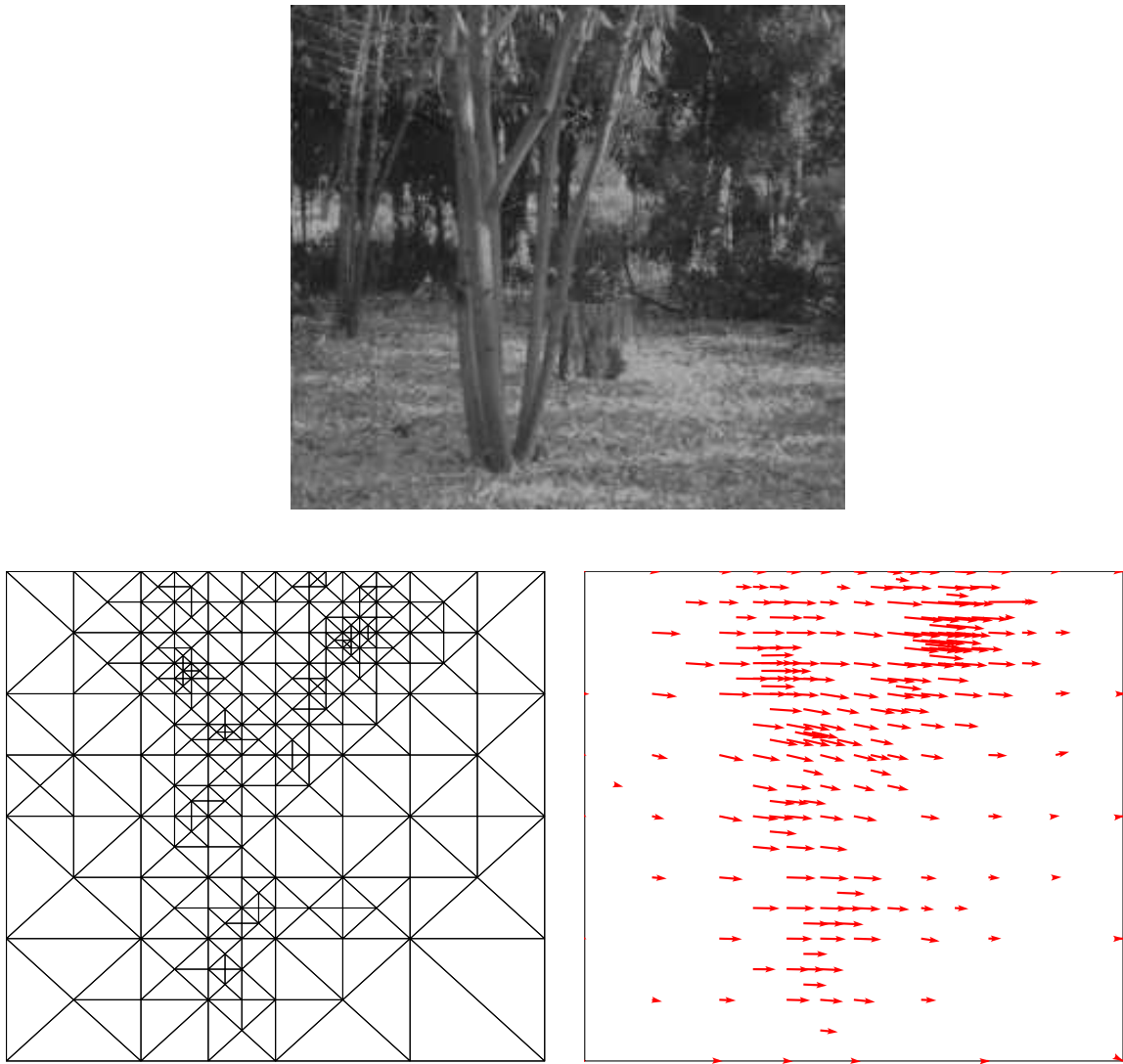
Figure 5: Flow computation on the **SRI Sequence**. We display a frame of the sequence, the adaptive mesh and the computed flow computed on this mesh.

Method	Average Error	Standard Deviation	Density
Horn & Schunck	32.81°	13.67°	100%
Anandan	31.46°	18.31°	100%
Singh	45.16°	21.10°	100%
Proposed Method	13.31°	3.18°	100%

Table 1: Comparison of various optical flow algorithms for processing the "square 2" image sequence (adapted from [1]).

pixels/frame), a car in the lower left, driving from left to right (3.0 pixels/frame), a van in the lower right, driving from right to left (3.0 pixels/frame) and a pedestrian in the upper left (0.3 pixels/frame). In figure 6 we show the first frame of the sequence and the associated mesh (motion threshold $w_-^{\mathcal{T}}$ is set to 1 pixels/frame, cell area threshold to 15 pixels). Figure 6 (bottom left and bottom right) shows a comparison between the solutions obtained by minimizing the quadratic functional (Eq.2, with $\alpha = 1$) and the non-quadratic one (Eq. 3). In this case, the motion is computed accurately for the white taxi and the van, while preserving the velocities discontinuities. The lower-contrast moving objects, for example the car in the lower left corner and the pedestrian are not characterized since the temporal image variations are very small and cannot be obtained from a temporal gradient computation based on two successive frames.

In Table 1 we list the results of some classical algorithms, on the "square2" image sequence. This synthetic example was used to quantify the accuracy of our model using the angular error measure of Barron *et al.* [1].

In the previous examples, the non uniform multigrid algorithm described in section 3 increases the numerical accuracy of the model (Eq. 6) and reduces its algorithmic complexity. This is due to the presence of objects having different velocities in the image sequence. This no longer true for image sequences with uniform motion (like "Otte's Sequence" [20]). For this kind of sequence the quadtree spline approach [26] seems to give a better accuracy/complexity ratio since the image is subdivided in regions having the same velocity.
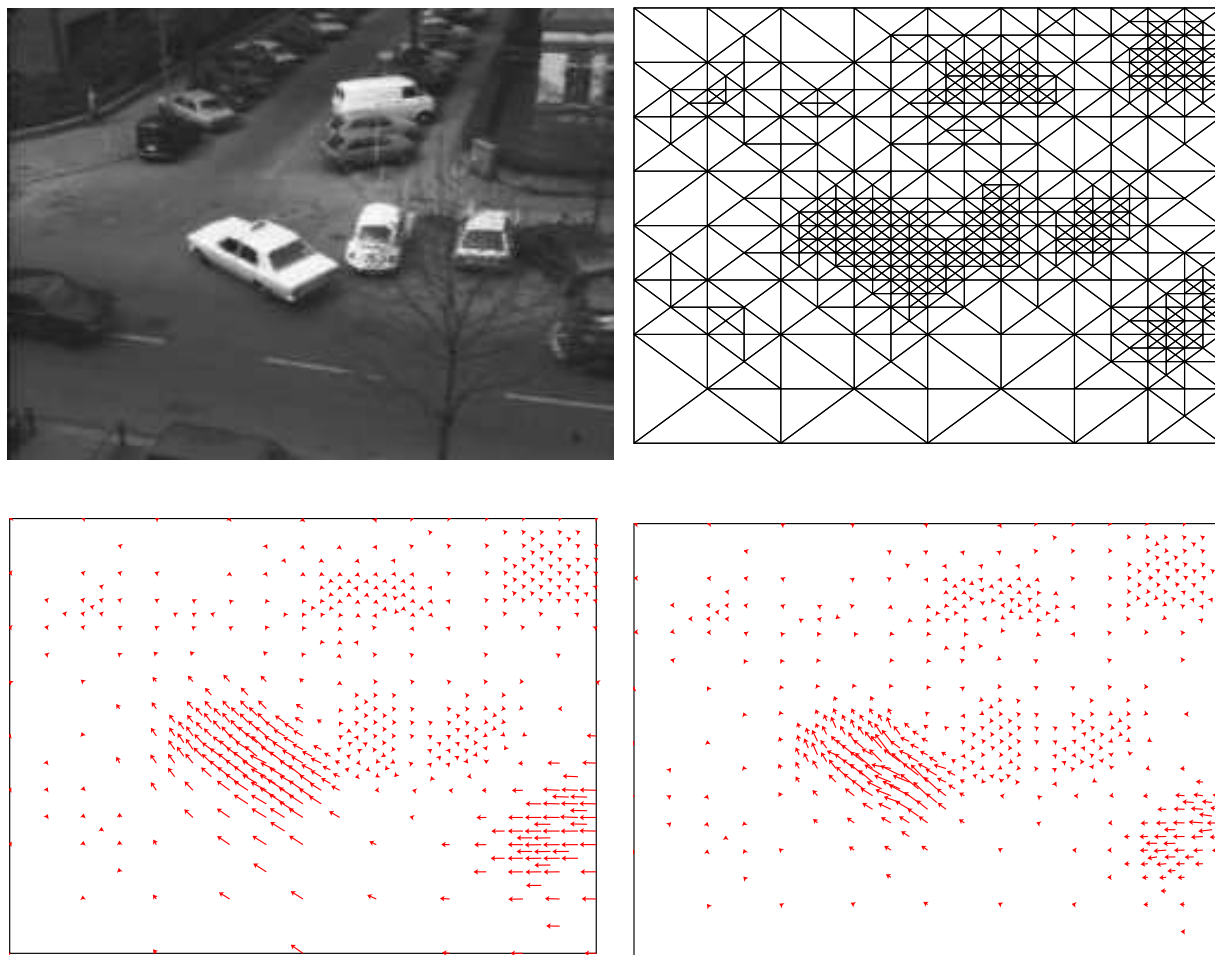
Figure 6: Flow computation on the "Hamburg Taxi Sequence". On the top the first frame of the sequence and the computed mesh are displayed. On the bottom are displayed the flow computed using a quadratic regularization technique (left) and the flow computed with the proposed approach (right).

4.2   Environmental Image Sequence

The previous experiments were reported in order to compare our optical flow method, based on a non uniform multigrid scheme, to the other ones and to evaluate its accuracy. Our main objective is to derive the surface ocean circulation from a sequence of Sea Surface Temperature measurements. These infra-red data are the most reliable ones for surface motion estimation and are daily available through the NOAA satellites. These measurements are corrupted by the presence of clouds. To overcome this problem, the data usually considered are composite images obtained by computing, at each pixel, the maximal value during a period of time. Figure 8 shows a seven days SST composite image. A frame of a high spatial and temporal resolution image sequence is displayed in Figure 7. This image concerns the confluence region near Argentina coast where a combined stream is formed by the Falkland northward flowing current (cold water), and southward flowing Brazilian current (hot water). This image sequence is a one day composite image sequence (since there are two NOAA satellites) acquired the first week of January 1988. Figure 7 displays the mesh subdivision based on the motion index w_- (Eq. 19) and the obtained displacement field characterizing the northward flowing current at at that period of the year.

Figure 9 displays the optical flow obtained by considering a non uniform multigrid with an unstructured mesh representation of the domain tessellation. This representation handles correctly the boundaries conditions associated to the PDE 4 when considering only mesh elements located on the ocean in order to reduce the computation time. We observe that the major streams of the Atlantic ocean are characterized. In figure 9 the Gulf stream and the confluence region (a combined stream formed by conjunction of different streams) near South America are closely related to the flow described in figure 10 representing the ocean circulation. Some of these flows occurs on the oceans surface and consequently can be tracked with SST image sequences.
We expect to compare the obtained displacement field to the one based on geostrophic motion, commonly used in physical oceanography. Another key point of our approach is to incorporate the obtained apparent motion field in a physical model modeling the interactions of land, atmosphere and oceans processes.

In the previous sections we dealt with some specific problems related to optical flow computation: flow discontinuities and non-uniform image tessellation. For both problems we presented
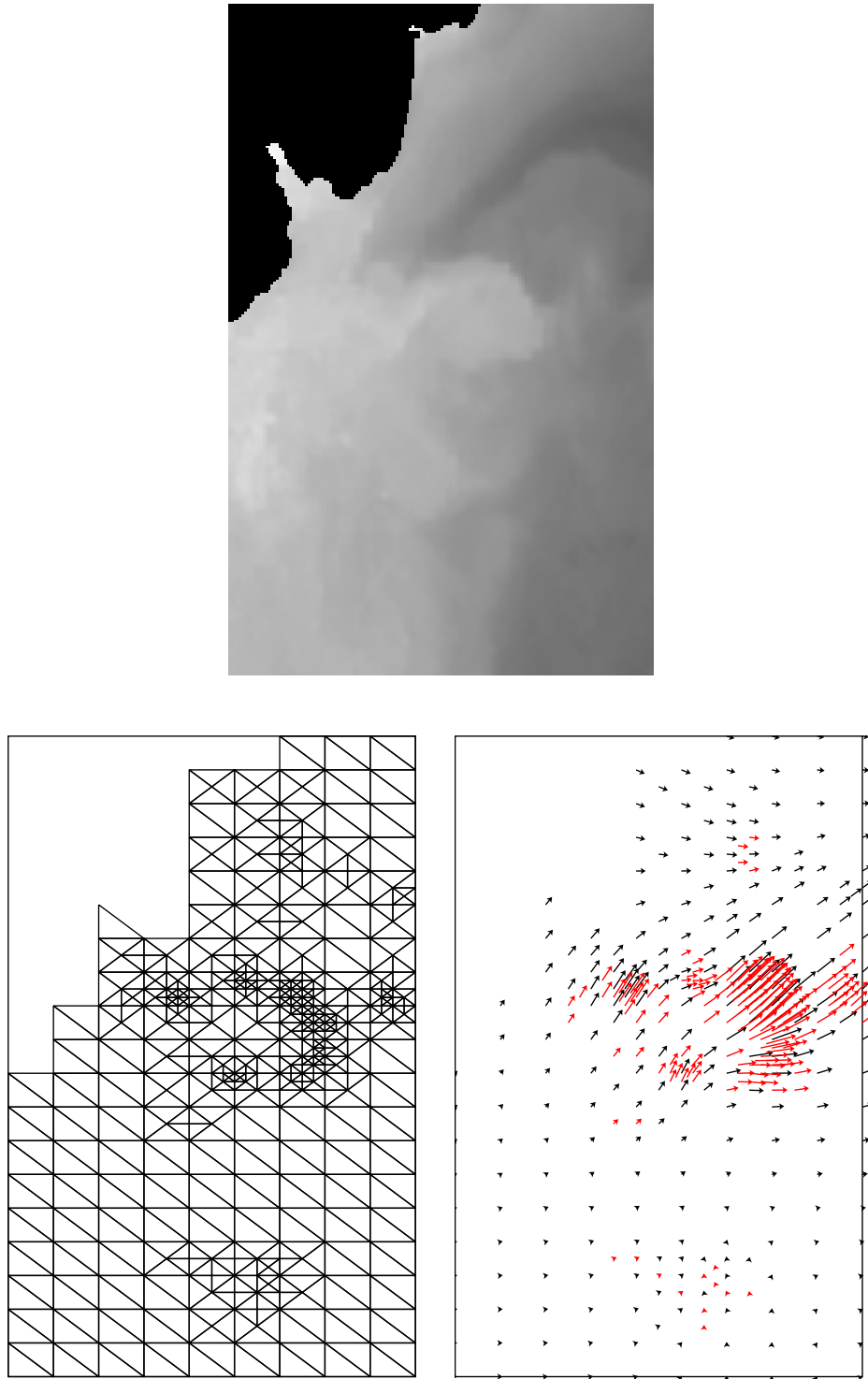
Figure 7: Illustration of the adaptive mesh approach for computing the optical flow from an image sequence. The upper figure displays a frame of the SST image sequence of the confluence region near Argentina coast. The two others figures show respectively the computed mesh based on the motion index and the obtained displacement field.
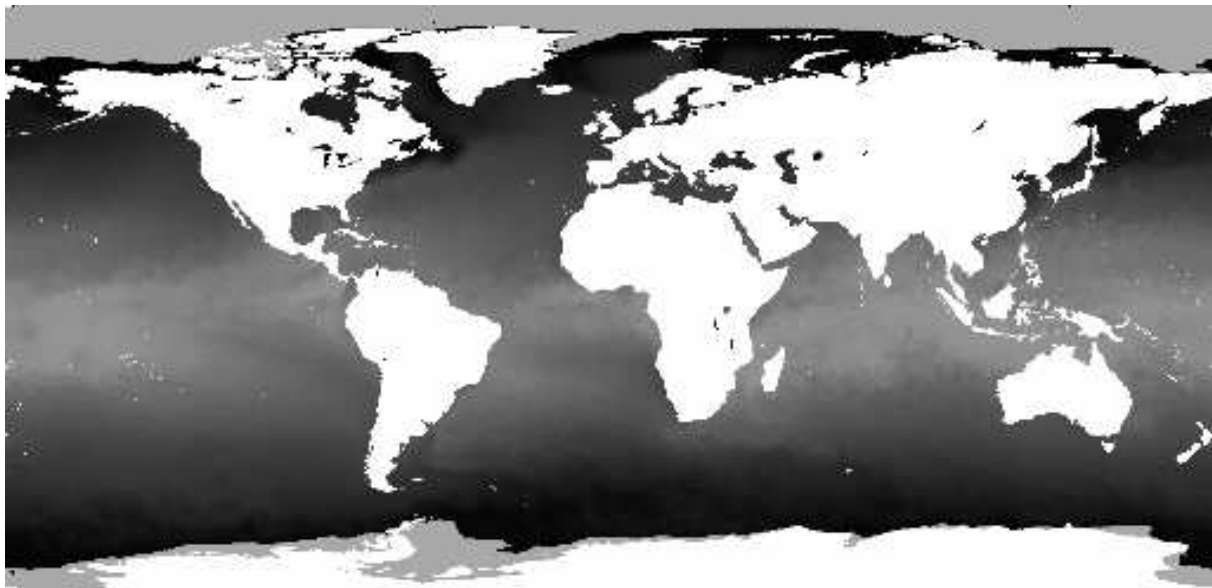
Figure 8: A seven days composite Sea Surface Temperature image (courtesy of NOAA/LODYC-Paris).

a solution allowing to improve optical flow accuracy and to reduce numerical complexity. This new framework, based on non uniform multiresolution and non quadratic regularization, allows to compute efficiently the apparent motion field over image sequences. Its computation gives a quantitative measure of the flow field at each image point (the use of a finite element method allows to reconstruct the solution over the whole image from a given tessellation). By processing Sea Surface Temperature and atmospheric image sequences we are also interested by the nature of motion since some phenomena, like vortices, are characterized through some specific patterns of the motion field. For this purpose we consider, in the following section, a characterization based on a phase portrait model. In the next two sections we briefly recall related work on flow pattern classification and present a new linear algorithm for arbitrary polynomial phase portraits and the classification of their stationary points.
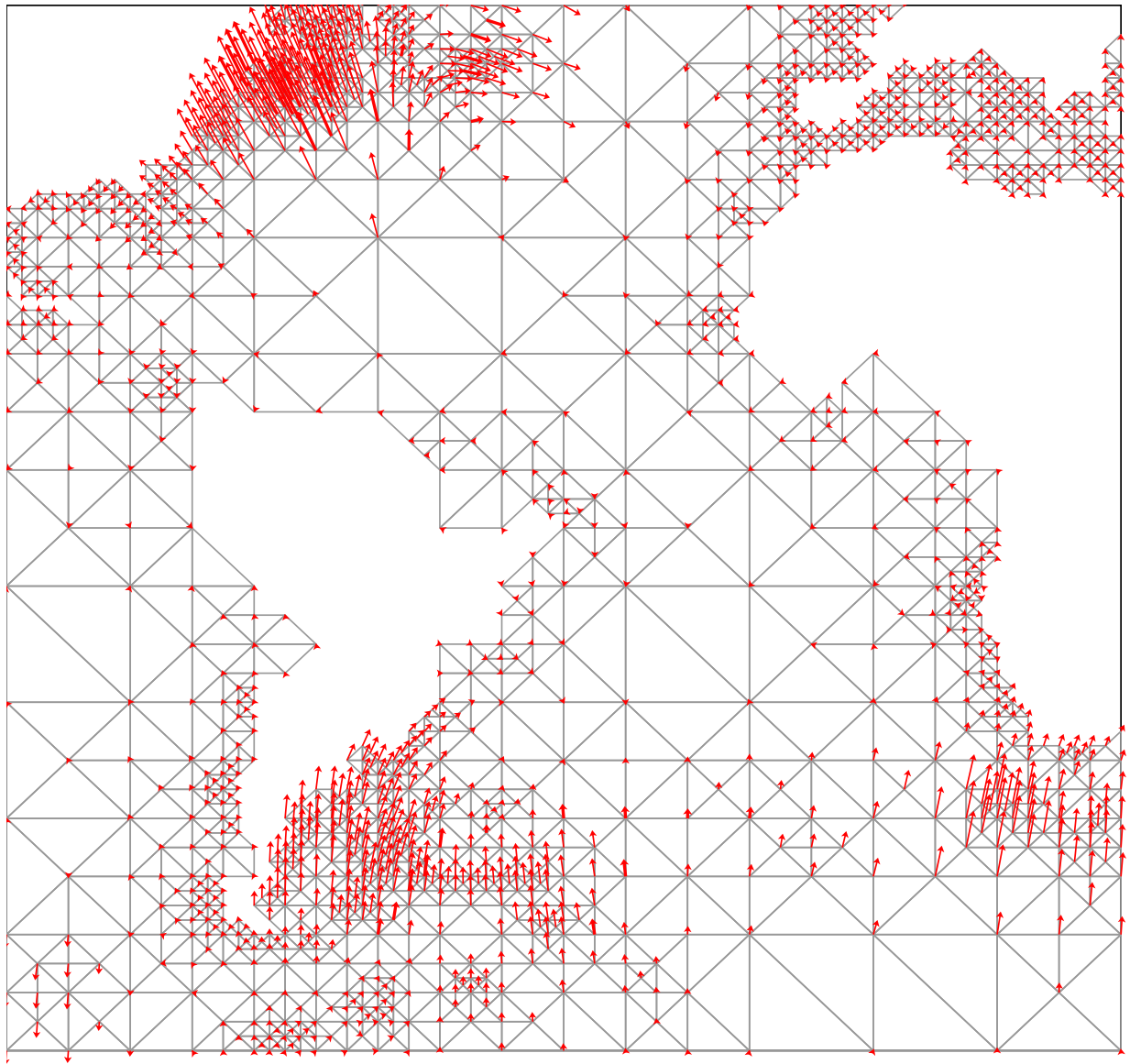
Figure 9: A global surface ocean circulation of the Atlantic Ocean obtained by the non quadratic optical flow method. The Gulf stream (in the upper left corner) is well characterized.
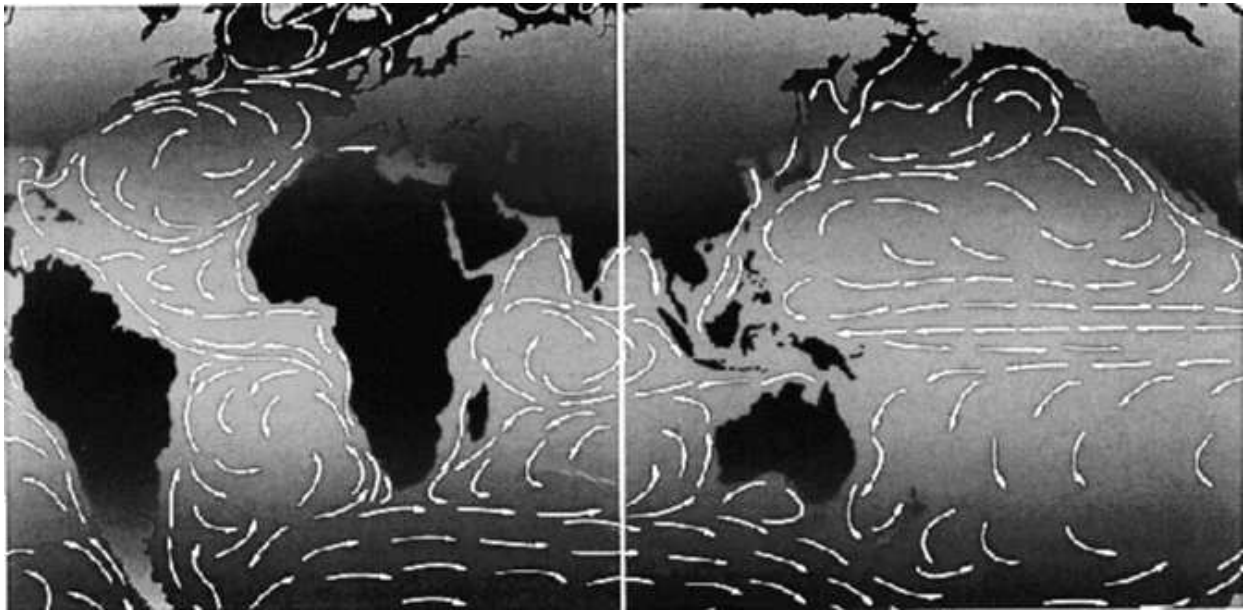
Figure 10: Ocean circulation model (courtesy of CNES-NASA).

5   Estimation of a Phase Portrait

The extraction of higher level descriptors from a flow field is naturally a very important task in studying fluid motion and vector analysis. In the forthcoming, we are mainly interested by vector analysis, some of the considered vector fields represent in fact a very complex fluid motion.

A classical approach is to use qualitative differential equations to characterize the orientation of the flow field by considering it as the velocity field of a particle in a dynamic system.

Let consider a particle governed by:

$$\begin{cases} \frac{dX}{dt} = P(x,y) \\ \frac{dY}{dt} = Q(x,y) \end{cases} \tag{21}$$

where $P(x,y)$ and $Q(x,y)$ are continuously differentiable functions. The particle trajectories are defined by the curve $(\varphi(t), \psi(t))$, $t > 0$, satisfying:

$$(\varphi\prime(t), \psi\prime(t)) = (P(\varphi(t), \psi(t)), Q(\varphi(t), \psi(t))). \tag{22}$$

Modeling the orientation flow field by a dynamic system allows to characterize the flow field through the particles trajectories and their stationary points.

Different works were led on linear phase portrait models [8, 21, 25] and their use for characterizing oriented texture fields. Recently, Zhong *et al* [30] proposed an application of linear phase portrait for structure's analysis in a fluid flow. The main drawback is that it can handle only one critical point. This limitation led to local [21] and global [25] implementations of the linear phase portrait model. Ford and Strickland [7] proposed a nonlinear phase portrait model allowing multiple critical points, but this model is computationally expensive and cannot be generalized to arbitrary polynomials. In the following, we propose a new approach for approximating an orientation field and characterizing the stationary points of the trajectories obtained from an arbitrary polynomial phase portrait. Furthermore this model is always linear, independently of the polynomial representation.

5.1   Distance Measure

In order to approximate a given flow field we have first, to define a distance measure which gives the similarity measure between two vectors. This measure is defined through the area subtended by the two vectors. Given two vectors A and B, a distance between them may be given by [10]:

$$dist(A, B) = \frac{1}{2} |A| |B| |sin(\theta)| \tag{23}$$

where θ is the angle subtended by the oriented segments. This distance represents the area of the triangle formed by these segments. Several authors [8, 21] used this measure to recover the six parameters of a linear phase model:

$$\begin{cases} \frac{dX}{dt} = ax + by + e \\ \frac{dY}{dt} = cx + dy + f \end{cases} \tag{24}$$

by locally minimizing the functional:

$$S_1 = \frac{1}{2} \sum_{i,j \in W} |A_{ij}|^2 |B_{ij}|^2 |sin(\theta_{1ij} - \theta_{2ij})|^2, \tag{25}$$

where W is the local region over-which the linear approximation is searched, θ_1 represents the linear model and θ_2 the vector field to approximate.

The use of the Levenberg-Marquardt method for minimizing such a non quadratic function, leads to a slow convergence rate.

In the following, we make use of another definition of the area subtended by two oriented segments that leads to the minimization of a quadratic functional. This definition of the distance is obtained from the norm of the cross product between the vectors A and B:

$$dist(A, B) = \frac{1}{2} |A \times B| . \tag{26}$$

Hence, considering a polynomial phase portrait model:

$$g(x, y) = \begin{cases} \frac{dX}{dt} = P(x, y) \\ \frac{dY}{dt} = Q(x, y) \end{cases} \tag{27}$$

where P and $Q \in Q_n(I\!\!R^2) = \left\{ p, \text{ st } p(x, y) = \sum_{i,j \leq n} a_{ij} x^i y^j \right\}$, we fit the model to the given orientation field $f = (f_1, f_2)^T$ (obtained from the optical flow field framework) by minimizing locally:

$$S_2(g) = \frac{1}{2} \sum_{i,j \in W} |f \times g|^2 , \tag{28}$$

where W is the neighborhood of the image point (i, j).

This criterion is easier to handle since it is quadratic. We prove that recovering the coefficients of the two polynomials P and $Q \in Q_n(I\!\!R^2)$ by minimizing S_2 amounts to an eigenvalue problem.

Let $X = (x^i y^j)_{i,j=0\ldots n}^T$ be the vector of basis functions of the space $Q_n(I\!\!R^2)$, the polynomial phase portrait model can be rewritten as:

$$g(x, y) = \begin{cases} \frac{dX}{dt} = P(x, y) = \sum_{i,j \leq n} a_{ij} x^i y^j = \Omega_a^T X \\ \frac{dY}{dt} = Q(x, y) = \sum_{i,j \leq n} b_{ij} x^i y^j = \Omega_b^T X \end{cases} \tag{29}$$

where $\Omega_a = (a_{ij})_{i,j \leq n}^T$ and $\Omega_b = (b_{ij})_{i,j \leq n}^T$ are $(n+1)^2$ dimensional vectors. The similarity measure S_2 can be reformulated as:

$$S_2(g) = \frac{1}{2} \sum_{i,j \in W} \left(\Omega_b^T X f_1 - \Omega_a^T X f_2 \right)^2 . \tag{30}$$

Let $B = \left(X^T f_2, -X^T f_1 \right)^T$ and $L = \left(\Omega_a^T, \Omega_b^T \right)^T$ the set of coefficients to be determined, the previous equation can be written as:

$$S_2(L) = \frac{1}{2} \sum_{i,j \in W} \left(B^T L \right)^2 . \tag{31}$$

An additional constraint must be added to ensure the uniqueness of the solution. Indeed, in order to recover a unique set of polynomial coefficients from an approximation of the orientation field, we have to consider a normalization constraint $L^T L = 1$. Finally, the similarity measure between a given orientation field $f = (f_1, f_2)^T$ and the model $g = \left(\Omega_a^T X, \Omega_b^T X \right)^T$ is given by the minimization under constraint of:

$$S_2(L) = \frac{1}{2} \sum_{i,j \in W} L^T B B^T L + \frac{1}{2} \lambda \left(L^T L - 1 \right) \tag{32}$$

A minimum of this functional is characterized by the derivative equations:

$$\begin{cases} \frac{\partial S_2}{\partial L} = B B^T L + \lambda L = 0 \\ \frac{\partial S_2}{\partial \lambda} = \frac{1}{2} \left(L^T L - 1 \right) = 0 \end{cases} \tag{33}$$

which lead to an eigenvector problem:

$$-B B^T L = \lambda L, \tag{34}$$

characterizing the polynomial coefficients represented by the vector L, with the normalization constraint: $L^T L = 1$.

This new formulation of the phase portrait similarity measure allows to derive a linear algorithm characterizing arbitrary polynomial portraits. The vector L representing the coefficients of the model in a given polynomial basis, is characterized by the eigenvector associated to the largest eigenvalue of the matrix $-B B^T$.

This definition of the similarity measure is a generalization of the approach proposed by Shu [25] based on the iso-tangent lines of a linear phase portrait model. However this model cannot handle multiple critical points and requires a particular processing for the orientations 0, $\pi/2$ and π.

5.2 Robustness in Case of Noisy Data

Local estimation of the vector L can be improved by using a weighted least-squares of the similarity measure (26). The weighting function gives more influence to the similarity measure at the center of the window but takes also into account the values in a given neighborhood. Such a

weighting is achieved by replacing the data vector $B = \left(X^T f_2, -X^T f_1 \right)^T$ by ωB, where ω is a weighting function satisfying $\sum\limits_{i,j \in W} \omega(i,j)^2 = 1$.

The local approximation of the orientation field is obtained by solving an eigenvector problem in $\mathbb{R}^{2(n+1)^2}$ (since $dim \left(Q_n \left(\mathbb{R}^2 \right) \right) = (n+1)^2$) :

$$-B\omega^2 B^T L = \lambda L. \tag{35}$$

over a centered window W. We use a Householder reduction and a QL algorithm to get the eigenvectors of the real symmetric matrix $B\omega^2 B^T$ [10]. The numerical complexity of the eigenvector problem (35) is $\mathcal{O}\left((2(n+1)^2)^3 \right)$.

5.3   Experiments

We have extensively tested our algorithm on various synthetic data. Figure 11 (left) is generated using a $Q_2(\mathbb{R}^2)$ polynomial phase portrait model with an additive gaussian noise ($\sigma = 0.6$). This example is very interesting since it has four stationary points and consequently cannot be processed with a global linear model. The approach described in section 5.2 allows to recover the initial phase model. The local approximation given in Figure 11 (right) illustrates the stability of the model for noisy data.

In the previous sections we showed how to fit an arbitrary polynomial model to a given orientation field. This orientation field can be obtained in different ways: oriented texture field [21], Fluid Mechanics or Optical flow techniques. Considering an optical flow field may be used to characterize coherent structures in a given displacement field. For instance, considering an apparent motion field from a Sea Surface Temperature (SST) or atmospheric image sequence should provide an evaluation of the surface ocean or atmospheric circulation and the study of the phase portrait of the associated orientation field may allow us to characterize structures like front and vortex. In the next section we propose a method for flow pattern classification of arbitrary phase portraits and an automatic localization of vortices in an atmospheric image sequence.
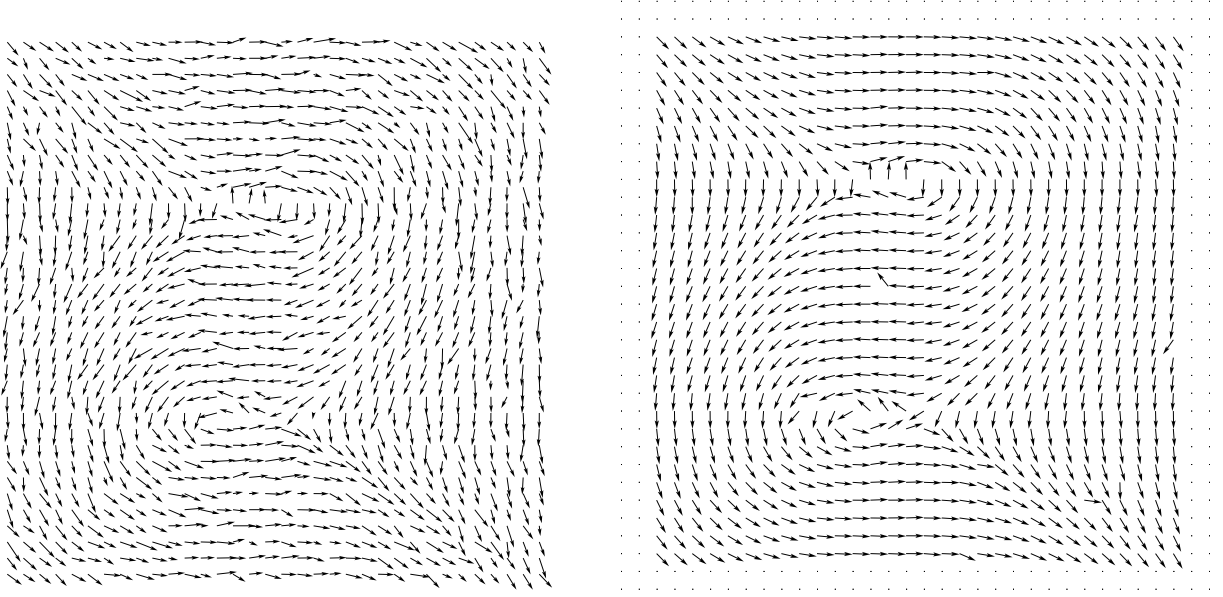
Figure 11: Approximation of a polynomial noisy ($\sigma = 0.6$) phase portrait model with a $Q_2(I\!\!R^2)$ polynomial.

6   Flow Pattern Classification

Analyzing a flow pattern consists in deriving a symbolic description from the model (27) fitted to the given local orientation field. In the case of optical flow, it would give a displacement information while in the case of fluid dynamic it will characterize the fluid velocity and the coherent structures in the flow. In the proposed approach, a displacement field is computed from an image sequence (SST or atmospheric images). The obtained optical flow characterizes the fluid motion. An illustration of such a approach is given by an image sequence of atmospheric infrared measurements. In this case the dynamic of clouds can be tracked with such image sequences. These data are used to derive the displacement field by using an optical flow method. The coherent structures are then obtained with a phase portrait model. Such an approach gives a qualitative description of the atmospheric circulation without using a complex physical model of the underlying phenomena (see Figure 13).

The symbolic description of the trajectory of the phase portrait model (Eq. 22) was extensively used in the case of a linear model. We will see in the next section that we obtain a complete analytical description of the particle trajectories governed by Eq. (24), from the solution of the linear system $AX + b = 0$, characterizing the stationary points of the system while the description of the flow is completely given by the eigenvalues of A [18]. This description is useful, since in the general case (*i.e.* arbitrary polynomials) a classification of the stationary points can be obtained from the linearization of the polynomial model.

6.1   The Linear Case

In this section we describe extensively the use of the algorithm in the case of a linear phase portrait model. In this case, the polynomials P and Q are in the space:

$P_1(I\!R^2) = \{p \text{ such that } p(x, y) = a_{00} + a_{10}x + a_{01}y\}.$

The vector basis of this space is $X = (1, x, y)^T$ and the linear model is given by :

$$\begin{cases} \frac{dX}{dt} = a_{00} + a_{10}x + a_{01}y = (a_{00}, a_{10}, a_{01}) X \\ \frac{dY}{dt} = b_{00} + b_{10}x + b_{01}y = (b_{00}, b_{10}, b_{01}) X. \end{cases} \quad (36)$$

A distance measure between the data $f = (f_1, f_2)^T$ at point (i, j) and the linear model is computed over a centered window $W = [i - N, i + N] \times [j - N, j + N]$. This local measure is given by equation (32) where $B = (f_2, xf_2, yf_2, -f_1, -xf_1, -yf_1)^T$ is a matrix with $(2N + 1)^2$ lines and 6 rows since the variables x and y spans the neighborhood W. Hence, the local minimization of the criteria (32) is equivalent to an eigenvalue problem in $I\!R^6$ where the solution is the eigenvector associated to the largest eigenvalue of $-B^T B$. Once we recovered at each point the coefficients of the linear model, particles trajectories near a fixed point x_f may be classified according to some characteristics of the eigenvalues of the matrix $A = \begin{bmatrix} a_{10} & a_{01} \\ b_{10} & b_{01} \end{bmatrix}$. Let λ_1 and λ_2 be the characteristic roots of A, we have the following classification :

- if λ_1 and λ_2 are real and distinct then x_f is a node,

  - if λ_1 and λ_2 are negative, x_f is a stable node,

  - if λ_1 and λ_2 are positive, x_f is an unstable node,

   – if $\lambda_1 \lambda_2 < 0$, x_f is a saddle point.

- if $\lambda_1 = \lambda_2 < 0$ or $\lambda_1 = \lambda_2 > 0$, x_f is a degenerate node,

- if $\lambda_1 = \lambda_2 = 0$, x_f is a singular node.

- if λ_1 and λ_2 are complex and $\lambda_1 = \overline{\lambda_2}$:

   – if $Re(\lambda_1) = 0$, x_f is a center,

   – if $Re(\lambda_1) < 0$, x_f is a stable focus,

   – if $Re(\lambda_1) > 0$, x_f is an unstable focus.

6.2   Elementary Critical Points in the General Case

In the general case we classify the stationary points of g through its linearization. This linearization holds only in the neighborhood of the stationary points.

Let consider the system (21) such that $P(x, y)$ and $Q(x, y)$ satisfy the conditions $P(0,0) = 0$, $Q(0,0) = 0$ and $\left| \dfrac{\partial(P,Q)}{\partial(x,y)} \right|_{(0,0)} \neq 0$. The system given by Eq. (21) can be rewritten by using the Jacobian $J = \dfrac{\partial(P,Q)}{\partial(x,y)}$:

$$\begin{cases} \dfrac{dX}{dt} = P(x,y) \\ \dfrac{dY}{dt} = Q(x,y) \end{cases} = J \begin{bmatrix} x \\ y \end{bmatrix} + \mathcal{O}_2 = \begin{bmatrix} a & b \\ c & d \end{bmatrix} \begin{bmatrix} x \\ y \end{bmatrix} + \mathcal{O}_2, \tag{37}$$

where $\mathcal{O}_2$ is a polynomial of the second order.

This linearization of the initial system allows to study the behavior of the particles trajectories only in the neighborhood of a critical point [15]. The behavior is the same as for the first order approximation (i.e. linear case) except when the characteristic roots are pure complex. In this case, we have a center or a focus [15].

In section 5 we showed how to locally fit the model to a given orientation field: at each point we consider a centered window over which the coefficients of the polynomial are recovered. Considering the first order approximation (37) in the neighborhood of a critical point gives a flow classification difficult to use since we have to locate critical points (i.e. to solve an arbitrary polynomial system) and to compute a flow classification based on the linearization (37). Instead we use the Index of a vector field to locate and characterize the stationary points.

6.3 Application of the Index to Differential Equations

Let $g = (P, Q)$ be a vector field defined over a Jordan curve J in the Euclidean plane, with no critical point on J. The index of g over J is proportional to the angular variation of the vector $g(M)$ (applied at $M \in J$) as M describes J. For the system (21), the index over an oriented Jordan curve J is given by:

$$\text{Index(J)} = \frac{1}{2\pi} \oint_J d\left(\arctan \frac{Q}{P}\right) = \frac{1}{2\pi} \oint_J \frac{P dQ - Q dP}{P^2 + Q^2}. \tag{38}$$

A classification of the flow field g may be obtained by computing the index over a small circle surrounding an isolated critical point. Since the computation of the stationary points of system (21) leads to the problem of solving a system of polynomials with an arbitrary degree, we choose to locally compute the index of $g = (P, Q)$ over the whole flow field data: At each point, a circle contained in the centered window W is considered for the following classification:

- The index of a focus, a center or a node is equal to $+1$,

- The index of a saddle point is -1.

Although this characterization is compendious, it characterizes the most important structures in a fluid flow field: stationary points. The index measure computed over all the flow, allows to obtain the critical points location without computing the roots of the system (21). Once these points are located, we may use the linearization technique described in section 6.2 to obtain a complete description of the flow field in the neighborhood of these stationary points.

6.4 Experiments

In this section we present the complete framework for processing an atmospheric infrared image sequence (Meteosat image) in order to compute cloud's motion and characterize cloud's vortices. The processing is done in two steps: A first step consists in computing the apparent motion field and the next one in characterizing flow patterns.

Figure 13 displays the optical flow obtained on a given frame. One can easily localize the vortex on the upper left corner of the figure from the flow structure. An approximation of this orientation field with a $Q_2(I\!\!R^2)$ polynomial phase portrait model and using the flow pattern classification
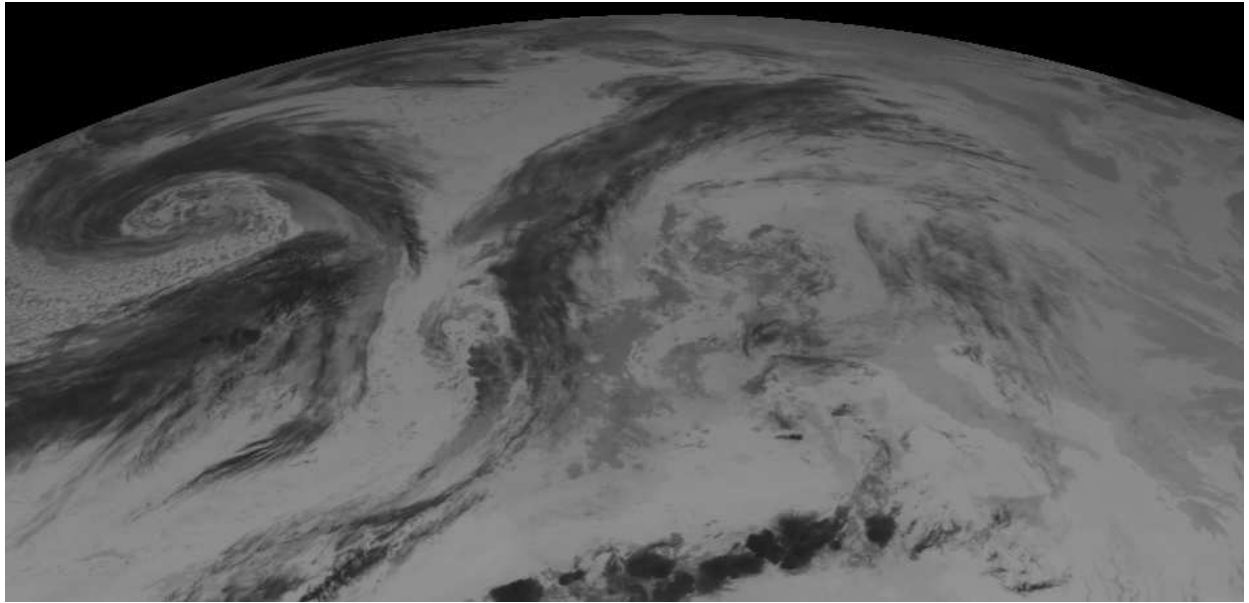
Figure 12: A frame of the infrared image sequence.

described in section 6.3 gives an accurate localization of the vortex. This processing was also applied to a SST image sequence in order to characterize ocean vortices [6].

The location of the detected vortex may further be used for a complete modeling of the vortex. Indeed, Herlin *et al* [11] use a geometric modeling of the vortex structure based on the location of vortex rolls. This approach is very stable and is used for tracking vortex shape in an image sequence. Another tracking model based on implicit functions was proposed by Yahia *et al* [29]. This model can handle topological changes of the structures being tracked. Finally, a pointwise tracking of the vortex shape can be achieved through a geometrical evolution model that enables to generate a surface interpolating the two successive contours of the object during its temporal evolution. This geometrical model defined by Berroir *et al* [2] may be viewed as a simplification of the true physical model of motion.
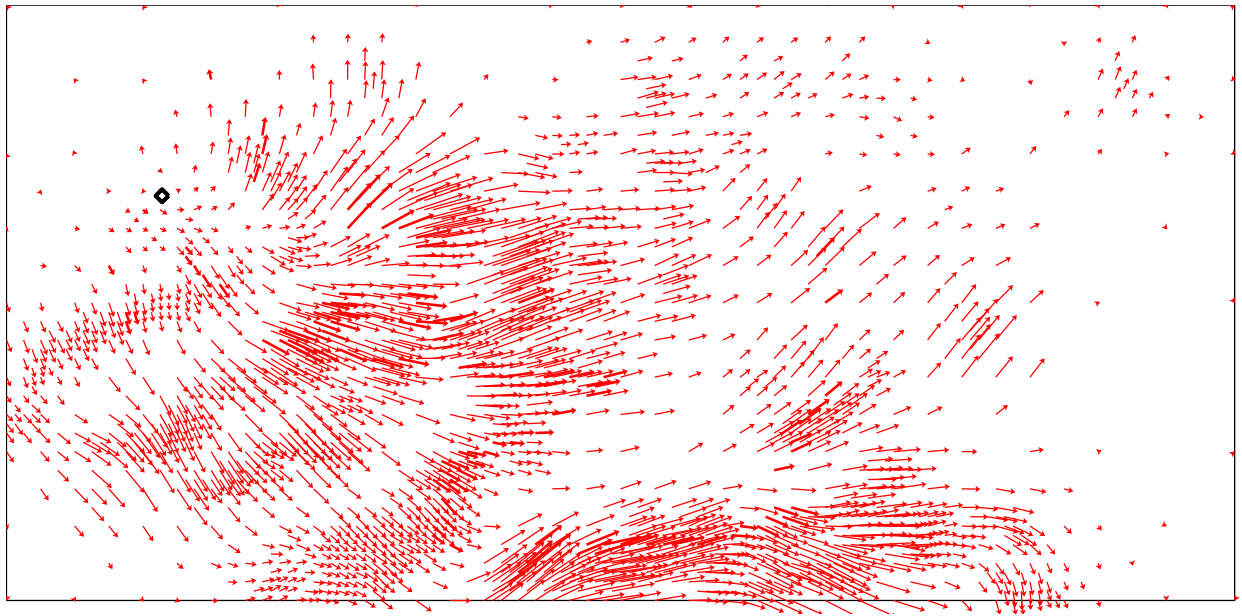
Figure 13: Optical flow characterizing clouds motion. The black quadrangle represents the vortex detected with the index approach. In this case, the given flow field (*i.e.* the optical flow) was approximated with a $Q_2(I\!\!R^2)$ polynomial.

7 Conclusion

In this paper we addressed some problems encountered in processing very large environmental image sequences representing the evolution of a physical phenomenon. The proposed framework represents an alternative to geostrophic methods based on a modeling of the underlying physical process.

The first part of the paper proposes a method for optical flow computation that preserves flow discontinuities and a non uniform multiresolution scheme allowing an efficient coarse to fine grid generation for optical flow computation. This method allows an important reduction of the algorithmic complexity while having a higher accuracy near moving structures.

The second part of the paper deals with the interpretation of the computed displacement field. Flow field interpretation is very important since it allows to detect coherent structures of the flow. Solving such a problem leads us to define a new flow field approximation method in order to consider arbitrary polynomial model which is more suitable for complex flow patterns approximation.

Furthermore, the presented model is always linear, independently of the polynomial representation. This processing is used on an atmospheric image sequence to characterize the vortices from the computed optical flow.

We are currently studying the comparison between the computer vision approach and the classical method used by oceanographic and atmospheric researchers which deal with more elaborated physical models.

Acknowledgements

References

[1] J.L. Barron, D.J. Fleet, and S.S. Beauchemin. Performance of optical flow techniques. *International Journal of Computer Vision*, 12(1):43–77, February 1994.

[2] J-P. Berroir, I. L. Herlin, and I. Cohen. Tracking highly deformable structures: a surface model applied to vortex evolution within satellite oceanographic images. In *EOS-SPIE Satellite Remote Sensing II*, 1995.

[3] M. J. Black. Recursive non-linear estimation of discontinuous flow fields. In *Third European Conference on Computer Vision*, pages 138–145, Sweden, May 1994. Springer-Verlag.

[4] M.J. Black and P. Anandan. Robust dynamic motion estimation over time. In *IEEE Proceedings of Computer Vision and Pattern Recognition*, pages 296–302, June 1991.

[5] P. G. Ciarlet. *The finite element methods for elliptic problems*. NORTH-HOLLAND, Amsterdam, 1987.

[6] I. Cohen and I. Herlin. Optical flow and phase portrait methods for environmental satellite image sequences. In *Proceedings of the Fourth European Conference on Computer Vision 1996*, Cambridge, April 1996.

[7] R. M. Ford and R. N. Strickland. Nonlinear phase portrait models for oriented textures. In *IEEE Proceedings of Computer Vision and Pattern Recognition*, pages 644–645, New-York, June 1993.

[8] R. M. Ford, R. N. Strickland, and B. A. Thomas. Image models for 2-D flow visualization and compression. *CVGIP: Graphical models and Image Processing*, 56(1):75–93, January 1994.

[9] R. Glowinski. *Numerical Methods for Nonlinear Variational Problems*. Springer-Verlag, New-York, 1984. Springer Series in Computational Physics.

[10] G. H. Golub and C. F. Van Loan. *Matrix Computations*. The Johns Hopkins University Press, London, second edition, 1989.

[11] I. Herlin, I. Cohen, and S. Bouzidi. Image processing for sequence of oceanographic images. *The Journal of Visualization and Computer Animation*, 1996. to appear.

[12] B.K.P. Horn and G. Schunck. Determining optical flow. *Artificial Intelligence*, 17:185–203, 1981.

[13] M. Irani, B. Rousso, and S. Peleg. Detecting and tracking multiple moving objects using temporal integration. In *Proceedings of the Second European Conference on Computer Vision 1992*, pages 282–287, May 1992.

[14] B. B. Kimia and K Siddiqi. Geometric heat equation and nonlinear diffusion of shapes and images. In *IEEE Proceedings of Computer Vision and Pattern Recognition*, pages 113–120, June 1994.

[15] S. Lefschetz. *Differential Equations: Geometric Theory*. Dover Publications, New York, second edition, 1976.

[16] P.L. Lions, J.M. Morel, and L. Alvarez. Image selective smoothing and edge detection by nonlinear diffusion. Technical Report 9046, CEREMADE, U.R.A. CNRS 749, Université Paris IX - Dauphine, 1990. Cahiers de Mathématiques de la Décision.

[17] J.R. Muller, P. Anandan, and J.R. Bergen. Adaptive-complexity registration of images. In *IEEE Proceedings of Computer Vision and Pattern Recognition*, pages 953–957, 1994.

[18] V. V. Nemytskii and V. V. Stepanov. *Qualitative Theory of Differential Equations*. Dover Publications, New York, 1989.

[19] W.J. Niessen and L.M.J. Florack A.H. Salden B.M. Romeny. Nonlinear diffusion of scalar images using well-posed differential operators. In *IEEE Proceedings of Computer Vision and Pattern Recognition*, pages 92–97, June 1994.

[20] M. Otte and H.-H. Nagel. Optical flow estimation: Advances and comparisons. In *Proceedings of the Third European Conference on Computer Vision 1994*, pages 51–60, May 1994.

[21] A. R. Rao and R. C. Jain. Computerized flow field analysis: Oriented textures fields. *IEEE Transactions on Pattern Analysis and Machine Intelligence*, 14(7):693–709, July 1992.

[22] J.B. Rosen. The gradient projection method for nonlinear programming. Part I: Linear constraints. *J. Soc. Indust. Appl. Math.*, 8(1):181–217, March 1960.

[23] L.I. Rudin, S. Osher, and E. Fatemi. Nonlinear total variation based noise removal algorithms. In *Ecoles CEA - EDF - INRIA; Problèmes Non Linéaires Appliqués: Modélisation Mathématique pour le traitement d'images*, pages 149–179, March 1992.

[24] H. Samet. *The Design and Analysis of Spatial Data Structures*. Addison-Wesley, 1989.

[25] C.-F. Shu and R.C. Jain. Vector field analysis for oriented patterns. In *IEEE Proceedings of Computer Vision and Pattern Recognition*, pages 673–676, Urbana Champaign, Illinois, June 1992.

[26] R. Szeliski and H.Y. Shum. Motion estimation with quadtree splines. Technical report, DEC Cambridge Research Lab, March 1995.

[27] M. Vasilescu and D. Terzopoulos. Adaptive meshes and shells: Irregular triangulation, discontinuities, and hierarchical subdivision. In *IEEE Proceedings of Computer Vision and Pattern Recognition*, pages 829–832, June 1992.

[28] A. Verri and T. Poggio. Motion field and optical flow: Qualitative properties. *IEEE Transactions on Pattern Analysis and Machine Intelligence*, 11(5):490–498, May 1989.

[29] H. Yahia, I. Herlin, and L. Vogel. Temporal tracking with implicit templates. Technical Report 2701, INRIA Rocquencourt, 1996. to appear.

[30] J. Zhong, T.S. Huang, and R.J. Adrian. Salient structure analysis of fluid flow. In *IEEE Proceedings of Computer Vision and Pattern Recognition*, pages 310–315, Seattle, Washington, June 1994.